

On the Influence of the Load Parasitics on the CM Conducted EMI of BLDC Motor Drives

Original

On the Influence of the Load Parasitics on the CM Conducted EMI of BLDC Motor Drives / Perotti, M.. - ELETTRONICO. - (2020). (20th IEEE International Conference on Environment and Electrical Engineering Madrid (Spain) 9-12 June 2020) [10.1109/EEEIC/ICPSEurope49358.2020.9160663].

Availability:

This version is available at: 11583/2834872 since: 2020-09-08T11:25:31Z

Publisher:

IEEE

Published

DOI:10.1109/EEEIC/ICPSEurope49358.2020.9160663

Terms of use:

This article is made available under terms and conditions as specified in the corresponding bibliographic description in the repository

Publisher copyright

IEEE postprint/Author's Accepted Manuscript

©2020 IEEE. Personal use of this material is permitted. Permission from IEEE must be obtained for all other uses, in any current or future media, including reprinting/republishing this material for advertising or promotional purposes, creating new collecting works, for resale or lists, or reuse of any copyrighted component of this work in other works.

(Article begins on next page)

On the Influence of the Load Parasitics on the CM Conducted EMI of BLDC Motor Drives

Michele Perotti

Department of Electronics and Telecommunications

Politecnico di Torino

Torino, Italy

michele.perotti@polito.it

Abstract

This paper analyzes the influence of the load parasitics on the conducted electromagnetic emissions, especially on their common mode component. The analyses have been performed on a BLDC motor driver, switched with bipolar PWM. According to the final installation of both the electronic module and the load, the prescribed test setup for the electromagnetic interference (EMI) measurements can vary. This modifies the parasitic element values and it can even worsen the emission level, when the load chassis is connected to the reference plane. In this paper, the effect of the load parasitic elements on the conducted emission is analyzed in details, and an equivalent model is derived and verified by simulation. Moreover, such simulations proved that the delay compensation technique can be used to counteract the EMI increase due to the load parasitics.

Index Terms

Conducted Emissions, common mode, load parasitics, BLDC.

I. INTRODUCTION

Nowadays, the electromagnetic compatibility of an electronic system with the surrounding environment, it is of fundamental importance. Modern electronic systems are usually equipped with power switching modules. Among them, the inverters used to drive permanent magnet motors, like the brushless DC ones, are widespread, especially in automotive field. The reason because this kind of motors is widely used, resides in their reliability and in their high power density [1]. Such motors are driven by a three-phase inverter, which is switched using pulse width modulation (PWM) in order to obtain the three trapezoidal driving waveforms.

The electromagnetic emissions, for the automotive modules, are regulated by the CISPR25 standard [2], which defines the test setup and it indicates the emission limits for both conducted and radiated emissions. Considering the conducted ones, and in particular their common mode (CM) component, these emissions are due mainly to the rising and falling edges of the inverter output voltages. The CM is caused by the disturbance current that propagates through the parasitic capacitances between the high dv/dt switching nodes and conductive plane, on which the electronic system is placed above during the emission measurement. The spectral component magnitude of such emissions depends on the shape of the output voltages and on the impedance present between the switching nodes and the reference plane [3]. To such impedance contribute both the parasitic capacitances referred to the inverter output nodes and the parasitic elements of the load [4], [5].

According to the standard and to the load installation in the final application, the load chassis can be either isolated from the reference plane or connected to it. This connection usually leads to increased CM emission, since the parasitic capacitance of the load is much greater with respect to the one of the inverter outputs. In order to reduce the emission several techniques can be used, with hardware [6]–[9] or software [10]–[13] approaches.

A possible solution to mitigate the EMI can be employed when the output voltages are switched by bipolar PWM. If the rising and falling edges of the output voltages are synchronized, no current flows back to the measurement instruments, since it recirculates locally through the parasitic capacitances. This is true if the output voltages are really complementary, and since it usually does not happen, because of delays in the propagation of the gating signals, the recently investigated delay compensation approach can be employed [14]. This compensation is performed using software, tightly modifying the PWM parameters.

This paper aims to analyze, and to verify by simulation, the influence of the load parasitics on the CM EMI spectrum, when the delay compensation technique is used. This has been pursued with an accurate model of the CM EMI, presented in Section 2, and a model of the load parasitics influence on the emission spectrum, investigated in Section 3. The simulations proving the accuracy of the model are reported in Section 4. The conclusions are drawn in Section 5.

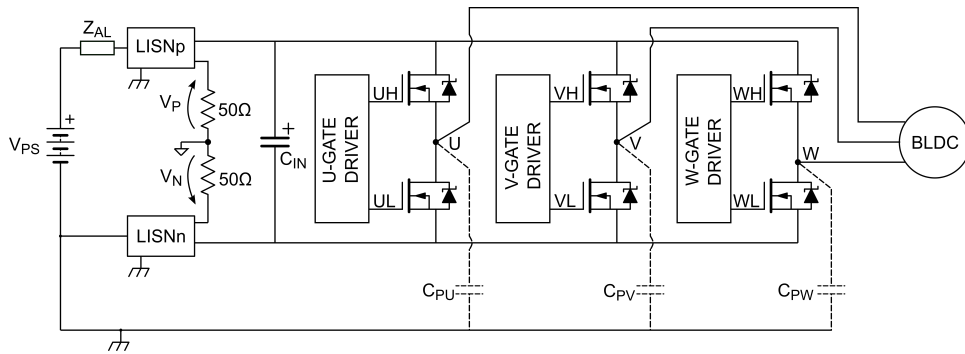


Fig. 1. Three-phase inverter circuit.

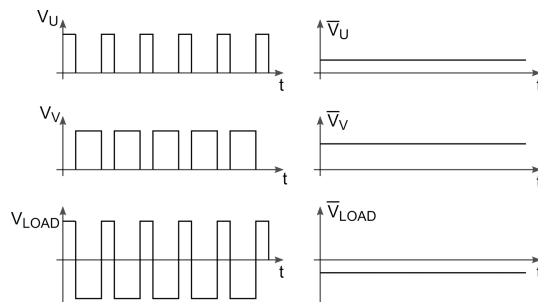


Fig. 2. Bipolar PWM: output waveforms and voltage on the load ($V_{LOAD} = V_U - V_V$).

II. CM CONDUCTED EMI OF BIPOLAR SWITCHED CIRCUITS

Among the switching circuits, the three-phase inverter is widely used in automotive field, and it can be employed to drive BLDC motors. This circuit is shown in Fig. 1. The BLDC motors are driven by six-step control. In each one of the six steps, only two out of three inverter outputs are modulated, while the third is left floating.

The three-phase inverter is supplied by a DC voltage source, V_{PS} , generated by a battery. The power supply is provided to the inverter through two LISNs, as prescribed in CISPR25 standard [2] for remotely grounded equipment.

Focusing on the inverter, each leg is composed of two n-MOS switches, whose gate terminal is controlled by a dual input-dual output gate driver. The output nodes of the inverter, U, V and W, provide the control waveforms to the BLDC motor.

The couple of active outputs in each step can be driven with different PWM strategies, but the bipolar PWM has been proven to be useful in reducing the common mode EMI [14]. An example of the output waveforms and their respective average voltages, for the control step in which the U and V outputs are active, is reported in Fig. 2.

Using the bipolar PWM, a positive average voltage is obtained using a duty cycle D greater than 0.5, while the negative one is obtained driving the other leg with complementary duty cycle, i.e. $(1 - D) < 0.5$. Therefore, the voltage on the load, $V_{LOAD} = V_U - V_V$, could reach values from $-V_{PS}$ to V_{PS} . In the following section, the contributions to the CM conducted emission are analyzed.

A. Analytical model of CM conducted EMI

Considering only the CM emissions, the equivalent circuit of the BLDC driver connected to the LISNs is shown in Fig. 3. For CM analysis, the two power supply nodes are connected together and the output voltages are modeled as a trapezoidal waveform voltage sources. Considering the step in which the U and V outputs are active, these generators, V_U and V_V drive the output parasitic capacitances C_{PU} and C_{PV} , respectively. The LISNs can be modeled, for the CM case, as an impedance $Z_{LISN} = 25 \Omega$.

In order to simplify the following analyses, the duty cycle D is fixed to 0.5. The same results can be drawn with other values of D .

The Fourier series of the outputs trapezoidal signal is expressed as [3]:

$$v(t) = \sum_{n=-\infty}^{\infty} V(jn\omega_0) e^{jn\omega_0 t}. \quad (1)$$

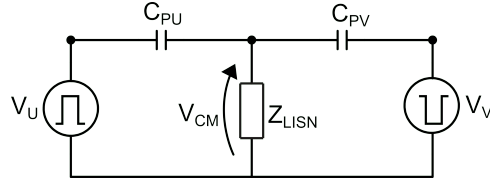


Fig. 3. Common mode equivalent circuit.

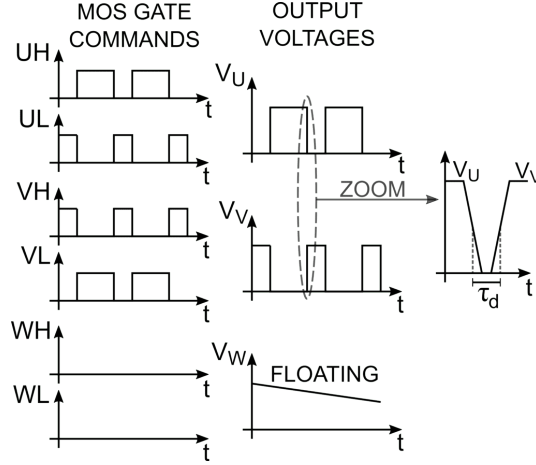


Fig. 4. Gate signals.

Since the two voltages V_U and V_V are complementary, they can be written as:

$$V_U(jn\omega_0) = V(jn\omega_0), \quad (2)$$

$$V_V(jn\omega_0) = V(jn\omega_0) \cdot e^{-jn\omega_0(\frac{T}{2})} \quad (3)$$

The major contributor to the CM emissions when a bipolar PWM is used, is the delay present between the active output waveforms. For this analysis, let's assume that the parasitic capacitances mismatch and transition time mismatch are null. In general, the output waveforms are not complementary one another since some delay due to the propagation of the gating signals from the microcontroller to the MOSFETs gates can be present. Among the causes of such a delay, the one introduced by the gate drivers is most relevant. Indeed, the commercial gate drivers are characterized by an input-output delay which could vary from tens to hundred of nanoseconds.

From these considerations, it is possible to evaluate how the analytical model for the CM emissions is influenced by the delay. Thus, the voltage generators at U and V nodes can be expressed as:

$$V_U(jn\omega_0) = V(jn\omega_0) \quad (4)$$

$$V_V(jn\omega_0) = V(jn\omega_0) \cdot e^{-jn\omega_0(\frac{T}{2} + \tau_d)} \quad (5)$$

where $V(jn\omega_0)$ is the Fourier series of the trapezoidal waveform and τ_d is the output delay, as presented previously and shown in Fig. 4.

The voltage at the LISNs CM output $V_{CM}(jn\omega_0)$ can be evaluated with the superposition of the effect of V_U and V_V :

$$\begin{aligned} V_{CM}(jn\omega_0) &= V(jn\omega_0) \cdot D(jn\omega_0) \cdot H(jn\omega_0) = \\ &= V(jn\omega_0) \cdot (1 + e^{-jn\omega_0(\frac{T}{2} + \tau_d)}) \cdot \frac{jn\omega_0 R C_P}{1 + 2jn\omega_0 R C_P} \end{aligned} \quad (6)$$

where $C_{PU} = C_{PV} = C_P$ and $R = Z_{LISN}$. It is possible to evaluate the contribution of τ_d on the CM emission, computing the magnitude of $D(jn\omega_0) = (1 + e^{-jn\omega_0(\frac{T}{2} + \tau_d)})$:

$$|D(jn\omega_0)| = |(1 + e^{-jn\omega_0(\frac{T}{2} + \tau_d)})| = \sqrt{2 - 2\cos(n\omega_0\tau_d)} \quad (7)$$

This term present a maximum magnitude equal to 2. When τ_d tends to 0, $D(jn\omega_0)$ tends to zero too and $V_{CM}(jn\omega_0)$ contribution on the emissions is canceled. Actually, other common mode contributions, like the asymmetries between the

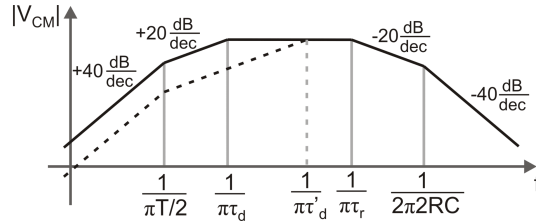


Fig. 5. CM voltage spectrum. The continuous line is derived with a time delay τ_d present between the output waveforms. When the delay is reduced from τ_d to τ'_d the spectrum is modified as the dashed line indicates.

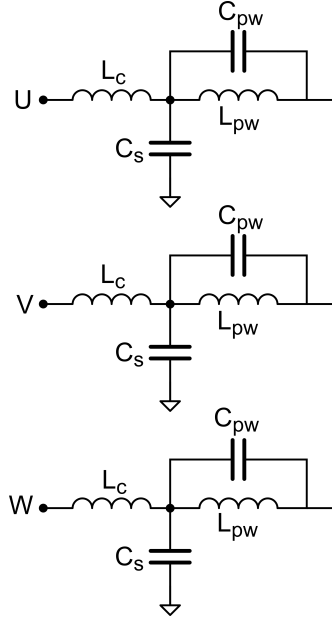


Fig. 6. High frequency model of a BLDC motor.

output waveforms, prevent it from happening. The D contribution can be approximated with its Taylor expansion. Therefore, the envelope of $|D(jn\omega_0)|$ for low frequencies has a slope of +20 dB/dec, while for higher frequencies it gives an oscillating contribution, whose maximum is equal to 6 dB. The corner frequency for this contribution can be found at $f_{pd} = 1/(\pi\tau_d)$.

The $|V_{CM}(jn\omega_0)|$ Bode diagram is shown in Fig. 5. The location of poles and zeros may change according to the waveform parameters values, i.e. rise-falling time, duty cycle, τ_d , etc. In such figure it is possible to see that, if the delay τ_d is reduced, the low frequency spectrum of the CM emissions is lowered.

The previous analysis does not take into account the parasitic elements of the load, which may contribute to the CM conducted emission. In the following section such contribution is modeled.

III. INFLUENCE OF THE LOAD PARASITICS

As shown in the previous section, the CM emission magnitude depends on the impedance present between the inverter output nodes and the LISNs. The parasitics of the load can modify significantly such an impedance. In particular, the load parasitic capacitances present between the load terminals and its chassis and the inductance of the interconnection cables can influence the magnitude of the CM conducted EMI. In order to evaluate the contributions to the CM conducted emissions of the BLDC parasitics, an high frequency model of the load, i.e. the BLDC motor, is needed [15], which in the conducted emission frequency range can be simplified as shown in Fig. 6. In this circuit, the main parasitics are present: the cable inductance L_C , the stator to chassis capacitance C_S , the interwinding capacitance of each phase C_{pw} and the phase inductance L_{pw} . The circuit that models the CM propagation path is shown in Fig. 7, where $V_{SW} = V(jn\omega_0) \cdot D(jn\omega_0)$. Since the phase inductance L_{pw} is usually high, it can be considered as an open circuit for the high frequency model.

When the load is well isolated from the reference plane, it is possible to conclude that the parasitic capacitance C_S can be neglected, since it presents a small and negligible value with respect to C_P . Therefore, the equivalent circuit for the CM propagation path is the one shown in the previous section, where only the parasitic capacitances C_P , referred to the output nodes of the driver, are considered.

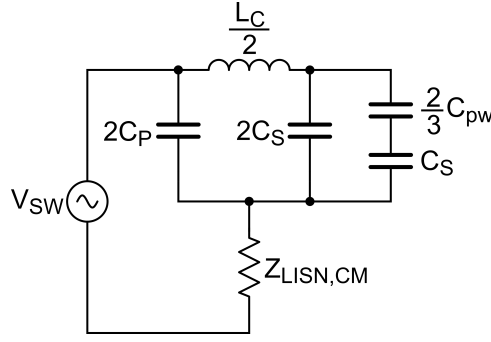


Fig. 7. CM propagation path considering the load parasitics.

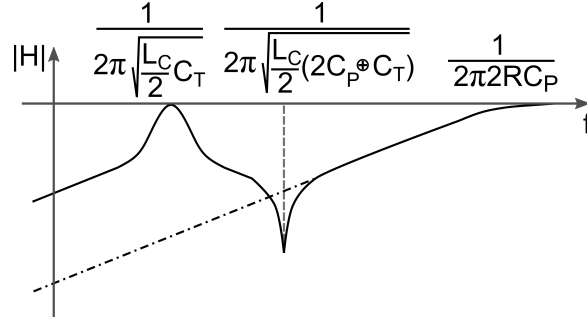


Fig. 8. Influence of the load parasitics on the transfer function H . The dashed dotted line is referred to the original case, in which the load parasitics can be neglected.

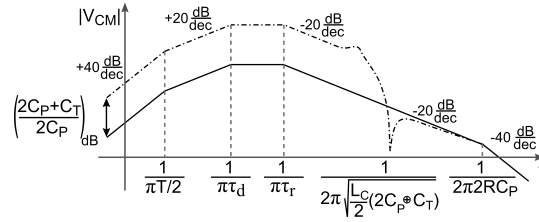


Fig. 9. Spectral envelope considering the load parasitic elements. When the load chassis is connected to the reference plane, the spectrum is increased as the dashed-dotted line indicates.

Instead, if the load chassis is connected to the reference plane, the load parasitics elements of the two active phases that have a major influence on the the CM disturbance propagation are the cable inductance $L_C/2$ and total load capacitance C_T comprising the winding-to-chassis capacitance $2C_S$, in parallel to a lower value capacitance, which is made of the interwinding capacitance and the one referred to the floating output:

$$C_T = 2C_S + \frac{2}{3}C_{pw} \oplus C_S \quad (8)$$

These two elements influence the CM spectra introducing two resonances: a series resonance between the cable inductance and the parasitic capacitance C_T , which generates a couple of complex conjugate poles, and a parallel one between the cable inductance and the harmonic sum of the two parasitic capacitances C_T and C_P , which gives rise to a couple of complex conjugate zeros. Therefore, the common mode propagation path, with the addition of the load parasitic elements, it is slightly modified. In Fig. 8 it is reported how the transfer function H is influenced by the load parasitics.

From the figure it can be seen that the parasitic capacitance of the load leads to an increased CM emission in the lower frequency range. This behavior is shown in Fig. 9.

The common mode emissions in the lower part of the spectrum are increased by the ratio between the total parasitic capacitance $2C_P + C_T$ and the isolated case parasitic capacitance $2C_P$.

Since it has been proven in [14] that a tight alignment of the output edges provides a reduction of the common mode emission, especially in the lower frequency range, the delay compensation can be used to counteract the effect of the load parasitics. In the following Section the analytical considerations made before are compared with SPICE simulations.

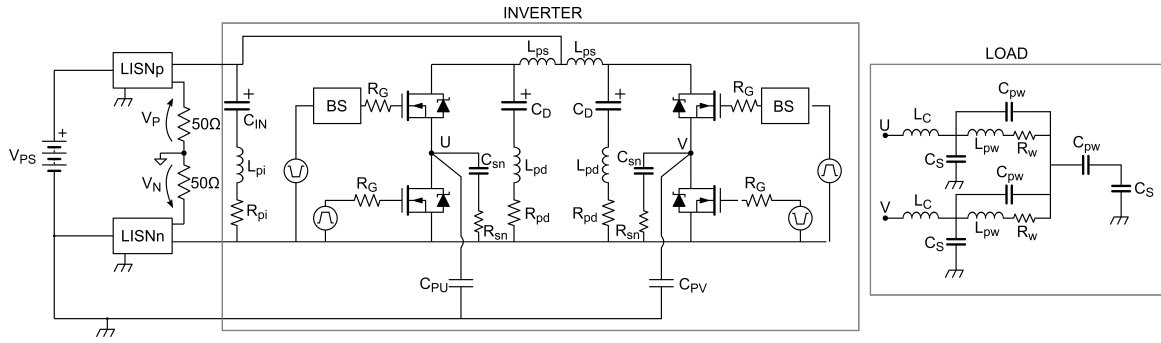


Fig. 10. Simulated schematic. The box BS represents the bootstrap circuit for the high-side MOS.

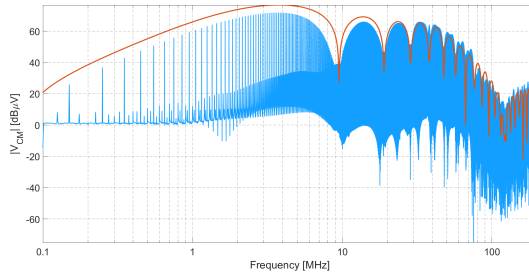


Fig. 11. Common mode emission spectrum, derived from simulation, and analytical spectral envelope. Motor chassis connected to the reference plane and $\tau_d \approx 100$ ns.

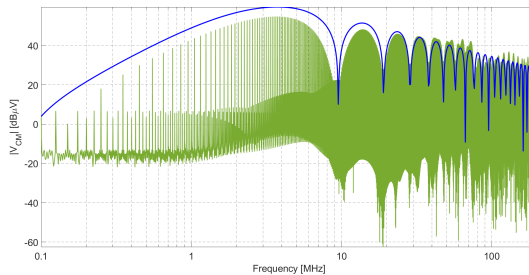


Fig. 12. Common mode emission spectrum, derived from simulation, and analytical spectral envelope. Motor chassis isolated and $\tau_d \approx 100$ ns.

IV. SIMULATION

The previous analysis has been verified by Spice simulations. Since only two out of three legs are active at a time, the three phase inverter can be simplified as a full bridge inverter. Moreover, the floating phase of the load can be modeled with its parasitic capacitances, since the inductance L_{pw} can be considered as an open circuit for the high frequency. The simulated inverter together with the load are shown in Fig. 10 and the parameter values are reported in Tab. IV. The nMOS switches model is provided by the manufacturer and the motor model values have been derived from measurements.

The simulated cases were related to two cases, representing two conditions for the load chassis connection to the reference plane: isolated and connected. In both cases, the output delay was set equal to $\tau_d \approx 100$ ns. In order to evaluate the influence of the delay on the spectrum, with the presence of the load parasitics, a third simulation was performed, with $\tau_d \approx 0$ ns and with the chassis connected to the reference plane. The simulations were performed, according to CISPR25, in the extended conducted emission frequency range, i.e. from 150 kHz to 108 MHz.

The results of the simulations, in which the delay is fixed at 100 ns and the chassis isolation is varied, are shown in Figs. 11 and 12. It can be seen that if the load chassis is not connected to the reference plane, the emissions are significantly reduced in the lower frequency range. On the same axes, the analytical model for the emission derived in the previous section is reported. It can be seen that it approximates well the behavior of the simulated spectra in the whole conducted emission frequency range. Comparing these two results, it is possible to see that, in the low frequency range, the ration between the two cases is coherent to the one predicted in Fig. 9.

According to the test setup, it is not always admitted to isolate the load from the reference plane. In these cases the emissions can be mitigated employing an EMI reduction technique, like the delay compensation one. This technique is able to reduce

TABLE I
SIMULATION PARAMETER VALUES

Parameter	Value	Parameter	Value
V_{PS}	12 V	R_G	3.3Ω
C_{IN}	4.7 mF	C_{sn}	4.7 nF
L_{pi}	20 nH	R_{sn}	3.9Ω
R_{pi}	$60 m\Omega$	C_D	$10 \mu F$
L_{ps}	50 nH	L_{pd}	10 nH
C_{PU}	6 pF	R_{pd}	$60 m\Omega$
C_{PV}	6 pF	C_S	43 pF / 1 pF
C_{pw}	9 pF	L_{pw}	$45 \mu H$
R_w	$9 m\Omega$	L_C	330 nH

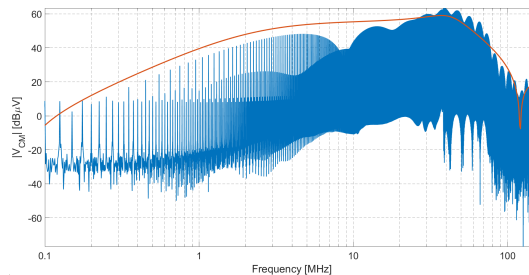


Fig. 13. Common mode emission spectrum, derived from simulation, and analytical spectral envelope. Motor chassis connected to the reference plane and $\tau_d \approx 0$ ns.

the CM EMI especially in the lower frequency range. The application of this technique to the not isolated case results in the spectrum reported in Fig. 13. It is possible to see that also in this case the model fits well the simulation results. Moreover, the emission level in this case is comparable to the one of the isolated case. This is obtained acting by software on the PWM parameters.

V. CONCLUSION

In this paper, the influence of the load parasitics on the CM conducted emission has been analyzed. A model of the CM EMI, when a bipolar PWM is used, has been derived considering also the load parasitics. From such a model, it turned out that the load cable inductances and the parasitic capacitances referred to the load chassis are the main contributors to the increase of the CM EMI. This model has been verified by simulation considering two cases: the first, where the load chassis is isolated from the reference plane and the second in which the chassis is connected to it. In the latter case, it has been verified that the emissions are increased proportionally to the ratio between the total parasitic capacitance of the non-isolated case and the one of the isolated case. The increment of the CM EMI level, due to the load parasitic effect, can be mitigated using the delay compensation technique. Indeed, it has been shown by simulation that the alignment of the output voltages reduces the EMI to a level which is comparable to the load isolated case.

REFERENCES

- [1] R. Krishnan, "Permanent Magnet Synchronous and Brushless DC Motor Drives", CRC Press, 2010.
- [2] IEC, "CISPR 25 - Vehicles, boats and internal combustion engines - Radio disturbance characteristics - Limits and methods of measurement for the protection of on board receivers", 2008.
- [3] C.R. Paul, "Introduction to Electromagnetic Compatibility. Second Edition.", Wiley, 2006.
- [4] X. Pan, R. Ehrhard and R. Vick, "An extended high frequency model of permanent magnet synchronous motors in hybrid vehicles," 10th International Symposium on Electromagnetic Compatibility, York, 2011, pp. 690-694.
- [5] Y. Wu, H. Li, W. Ma, M. Dong and Q. Zhong, "High-frequency Model of Permanent Magnet Synchronous Motor for EMI prediction in Adjustable Speed Drive System," 2018 IEEE International Power Electronics and Application Conference and Exposition (PEAC), Shenzhen, 2018, pp. 1-6.
- [6] R.L. Ozenbaugh and T.M. Pullen, "EMI Filter Design. Third Edition.", CRC Press, 2012.
- [7] D. Xu *et al.*, "An Active EMI Choke for Both Common- and Differential- Mode Noise Suppression", in IEEE Transactions on Industrial Electronics vol. 65, n. 6, pp. 4640-4649, 2018.
- [8] B. Narayanasamy and F. Luo, "A Survey of Active EMI Filters for Conducted EMI Noise Reduction in Power Electronic Converters," in IEEE Transactions on Electromagnetic Compatibility, vol. 61, no. 6, pp. 2040-2049, Dec. 2019.
- [9] X. Zhang, M. Khodabandeh, M. Amirabadi and B. Lehman, "A Simulation-Based Multifunctional Differential Mode and Common Mode Filter Design Method for Universal Converters," in IEEE Journal of Emerging and Selected Topics in Power Electronics, vol. 8, no. 1, pp. 658-672, March 2020.
- [10] R. Gamoudi, D. Elhak Chariag and L. Sbita, "A Review of Spread-Spectrum-Based PWM Techniques—A Novel Fast Digital Implementation," in IEEE Transactions on Power Electronics, vol. 33, no. 12, pp. 10292-10307, Dec. 2018.
- [11] Y. Chen, M. Yang, J. Long, D. Xu and F. Blaabjerg, "A DDS-Based Wait-Free Phase-Continuous Carrier Frequency Modulation Strategy for EMI Reduction in FPGA-Based Motor Drive," in IEEE Transactions on Power Electronics, vol. 34, no. 10, pp. 9619-9631, Oct. 2019.

- [12] J. Chen, D. Jiang, Z. Shen, W. Sun and Z. Fang, "Uniform Distribution Pulsewidth Modulation Strategy for Three-Phase Converters to Reduce Conducted EMI and Switching Loss," in *IEEE Transactions on Industrial Electronics*, vol. 67, no. 8, pp. 6215-6226, Aug. 2020.
- [13] M. Blank et al., "Digital Slew Rate and S-Shape Control for Smart Power Switches to Reduce EMI Generation", in *IEEE Transactions on Power Electronics* vol. 30, n. 9, pp. 5170-5180, 2015.
- [14] M. Perotti and F. Fiori, "Investigating the EMI Mitigation in Power Inverters Using Delay Compensation," in *IEEE Transactions on Power Electronics*, vol. 34, no. 5, pp. 4270-4278, May 2019.
- [15] F. Diouf, F. Leferink, F. Duval and M. Bensetti, "Wideband Impedance Measurements and Modeling of DC Motors for EMI Predictions," in *IEEE Transactions on Electromagnetic Compatibility*, vol. 57, no. 2, pp. 180-187, April 2015.